Hindawi
Mathematical Problems in Engineering
Volume 2018, Article ID 2717129, 16 pages
https://doi.org/10.1155/2018/2717129

Research Article

Proportional Load Sharing and Stability of DC Microgrid with Distributed Architecture Using SM Controller

Muhammad Rashad,[1] **Uzair Raoof**,[2] **Muhammad Ashraf**,[1] **and Bilal Ashfaq Ahmed**[2]

[1]*Department of Electrical Engineering, Capital University of Science and Technology (CUST), Kahuta Road, Express Highway, Islamabad 44000, Pakistan*
[2]*Department of Electrical Engineering, The University of Lahore (UOL), Defense Road, Lahore 54000, Pakistan*

Correspondence should be addressed to Muhammad Rashad; muhammad.rashad@ee.uol.edu.pk

Received 7 September 2017; Revised 15 November 2017; Accepted 29 November 2017; Published 8 January 2018

Academic Editor: Rafael Morales

DC microgrids look attractive in distribution systems due to their high reliability, high efficiency, and easy integration with renewable energy sources. The key objectives of the DC microgrid include proportional load sharing and precise voltage regulation. Droop controllers are based on decentralized control architectures which are not effective in achieving these objectives simultaneously due to the voltage error and load power variation. A centralized controller can achieve these objectives using a high speed communication link. However, it loses reliability due to the single point failure. Additionally, these controllers are realized through proportional integral (PI) controllers which cannot ensure load sharing and stability in all operating conditions. To address limitations, a distributed architecture using sliding mode (SM) controller utilizing low bandwidth communication is proposed for DC microgrids in this paper. The main advantages are high reliability, load power sharing, and precise voltage regulation. Further, the SM controller shows high robustness, fast dynamic response, and good stability for large load variations. To analyze the stability and dynamic performance, a system model is developed and its transversality, reachability, and equivalent control conditions are verified. Furthermore, the dynamic behavior of the modeled system is investigated for underdamped and critically damped responses. Detailed simulations are carried out to show the effectiveness of the proposed controller.

1. Introduction

Microgrids are a modern form of distribution systems which can function autonomously or in combination with a main supply grid. Microgrids can operate in a low or medium voltage range and generate their own power, that is, renewable sources along with energy storage, nonrenewable sources, and power electronic (PE) controlled loads [1]. The unique property of microgrids is that they can work in islanded mode under faulty conditions, which increases the reliability of the power supply [2–4]. In AC microgrids, the distribution system is AC. AC microgrids operation and control have been exhaustively discussed in the literature [5, 6]. DC microgrids are paid attention from researchers due to the following advantages:

(1) Most of the renewable sources are inherently DC or DC friendly. So, the integration of these sources with a DC microgrid is easy as there is no requirement of frequency synchronization circuits.

(2) In DC microgrids, reactive power compensators are not required. Hence, their control will be relaxed as power flow controllers are not required.

(3) As DC electronic loads dominate today, the unnecessary AC-to-DC converters are not required in DC microgrids. This will directly affect system cost and efficiency.

(4) Skin effect problems are absent in DC microgrids.

A general DC microgrid arrangement [7, 8] connecting different sources and loads is shown in Figure 1. To integrate dissimilar elements, PE converters (DC-to-DC, AC-to-DC, etc.) are included among sources, energy storage, and microgrids.

Distributed generation can be connected to the DC microgrid through power PE converters in a parallel configuration. It is required to find efficient control to coordinate

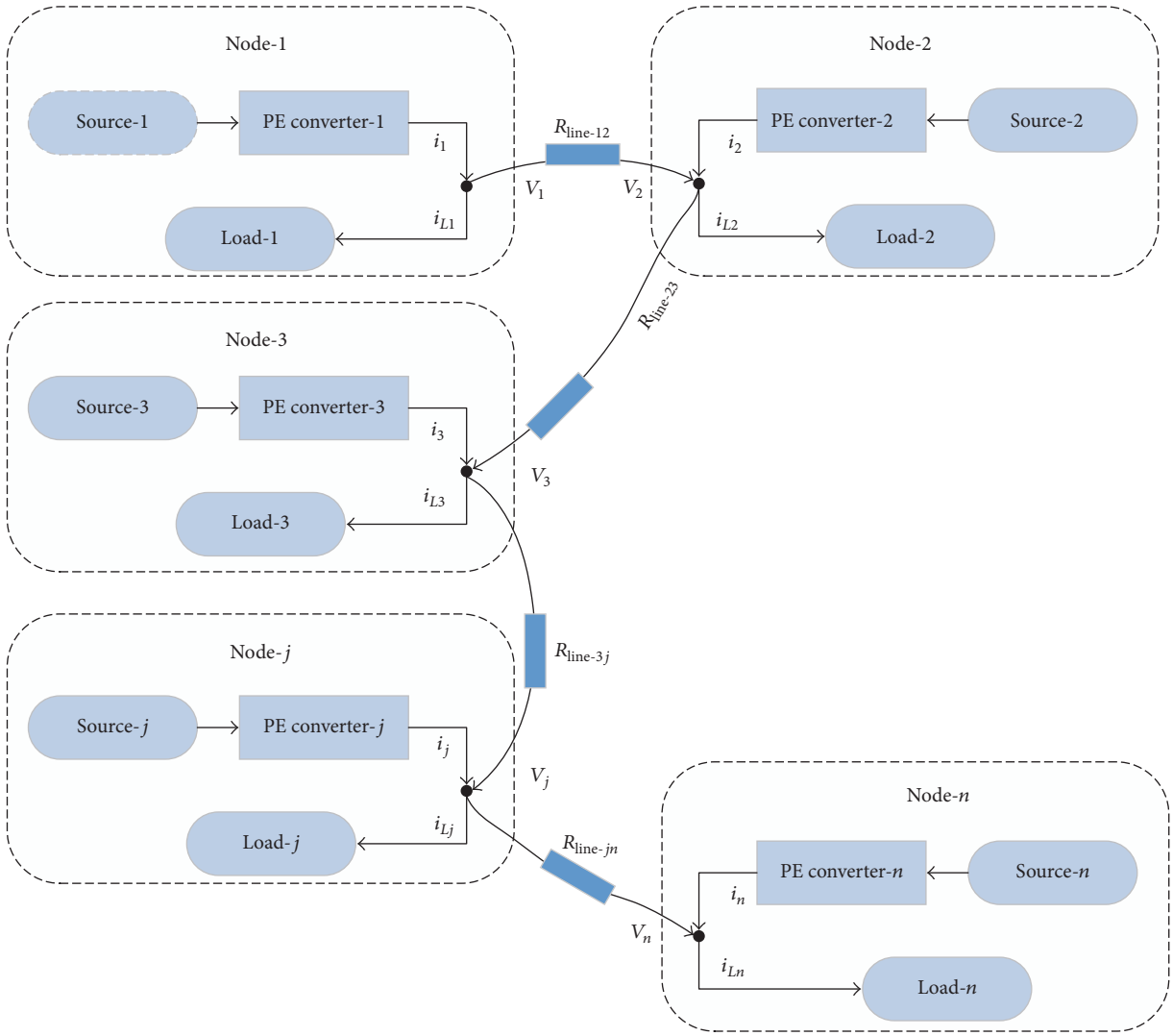

Figure 1: General DC microgrid arrangement [8].

among various sources, loads, and energy storage. The key concerns of the parallel connected converter are as follows: the first concern is the stability of the DC microgrid as electronic loads are very sensitive to voltage deviation. Another concern is load sharing among various sources [7–9]. However, it is the nature of sources that only one unit can establish the voltage level in a paralleling system. The reason is, the output resistances of the power sources are extremely low. Thus, even a small difference in the output voltage between the paralleled sources will cause the one that is a few mV higher to hog all the current. The lower the output voltage of the module is, the more severe this problem is [10].

To address the aforementioned challenges, different control schemes for DC microgrids are reported in [7, 10–16]. Commonly, these control schemes can be categorized as centralized and decentralized control [10–21]. In centralized control, the controller collects system data using a high bandwidth communication link, schedules the tasks based on the collected information, and directs control decisions [12, 16–18]. However, if the communication link fails, this will degrade the system performance and reliability. Communication failure problems can be avoided in decentralized control (droop control) [13, 14, 19, 22]. In this type of control, PE converters operate on physical measured quantities. But the improvement is achieved at the cost of partial stability and losing optimum operation due to the lack of operational information and status of the other converters [23, 24]. In [25–29], droop control for AC microgrids is reported. Their extensive use in conventional AC systems made them appealing to be used in DC microgrids [30–32].

Linear proportional integral (PI) controllers are used to realize the abovementioned control schemes for proportional load sharing and stability of DC microgrids [30–32]. Despite the easy implementation of these controllers, they suffer poor sharing. In many cases, the stability of PI controllers cannot be ensured [33, 34]. Since PI controllers are linear type controllers, the control parameters of these controllers cannot be optimized as they are tuned for specific load conditions. Further, they also exhibit a slower dynamic response [35]. Hence, using these controllers for load sharing is not desirable.

Sliding mode control (SMC) for proportional load sharing and stability of DC microgrids is proposed in this paper. SMC for microgrid type systems is reported in [9, 36–40]. SM is a controller which is used for variable structure systems [36]. It is a nonlinear controller which shows robust behavior to the matched uncertainties. The SM controller can be easily implemented using integrated circuits. Hence, the SM controller is proposed for proportional load sharing and stability of DC microgrids.

Section 2 deals with the load sharing control schemes used in DC microgrids. Further, a system model and its analysis through the SM controller are presented. Furthermore, this section deals with system stability and dynamic behavior design. Detailed simulation studies are performed in Section 3. Section 4 concludes this paper.

2. Load Sharing Control in DC Microgrids

The objective of the control in DC microgrids is to achieve load sharing and maintain precise voltage regulation among the sources. The sharing control can be categorized into the following types.

2.1. Centralized Control. In this type of control, the controller collects system data using a communication link and directs control decisions. This type of control scheme is reported in [12, 16–18] and is shown in Figure 2. The PE converter of each source contains primary control and inner voltage and current control. Centralized control gives directions and control decisions to the other primary controllers. The voltage of the DC microgrid is communicated to the central controller, where it is compared with the reference voltage. The error produced is transferred to the PI controller whose output is communicated to the primary controller of each source as shown in Figure 2. However, if a single point failure occurs, this will degrade the system performance and reliability. Hence, using centralize control for load sharing and voltage regulation in DC microgrids is not attractive.

2.2. Decentralized Control. Single point failure problems can be avoided in decentralized control (droop control) [13, 14, 19, 22]. In this type of control, PE converters operate on local physical measured quantities. This does not require a separate central controller. Decentralized control sets the values for droop control which derives the inner voltage and current control of the PE converters as shown in Figure 3.

Droop control cannot achieve load sharing and voltage regulation simultaneously. Limitations of the droop control are examined below.

2.2.1. Current Sharing Inaccuracy. Current sharing will be affected due to the voltage error in parallel connected DC-to-DC converters. This problem becomes challenging due to the extra voltage drop across the line connecting parallel sources or when the characteristics of different sources are not the same. Hence, current sharing among various sources is deteriorated. To analyze this problem, a DC microgrid with two sources is shown in Figure 4, where each source is modeled by its Thevenin equivalent circuit.

The droop control used in DC systems can be expressed as

$$v_{sj} = v_s - i_{\mathrm{dc}j} R_{dj} \quad \text{where } j = 1, 2, \tag{1}$$

where v_{sj}, v_s, $i_{\mathrm{dc}j}$, and R_{dj} are node voltage, source voltage, source current, and virtual resistance of each source, respectively. The virtual resistance defined in (1) is equal to the output resistance and the output voltage of each source is equal to v_s, as shown in Figure 4. Consider the load is drawing rated current and the system has reached a steady state. The following can be derived from Figure 4:

$$v_{\mathrm{load}} = v_s - i_{\mathrm{dc}1} R_{d1} - i\mathrm{dc}_1 R_{\mathrm{line}1} \tag{2a}$$

$$v_{\mathrm{load}} = v_s - i_{\mathrm{dc}2} R_{d2} - i\mathrm{dc}_2 R_{\mathrm{line}2}. \tag{2b}$$

After simplification, these equations can be written as

$$\frac{i_{\mathrm{dc}1}}{i_{\mathrm{dc}2}} = \frac{R_{d2}}{R_{d1}} + \frac{R_{\mathrm{line}2} - \left(R_{d2}/R_{d1}\right) R_{\mathrm{line}1}}{R_{d1} + R_{\mathrm{line}1}}. \tag{3}$$

The above equation shows that, in droop controlled DC grids, the current of both sources is inversely proportional to their virtual resistance. Usually, it is assumed that DC microgrids are small-scale grids and the connecting lines will contain resistance of a small value. Hence, virtual resistance R_{dj} can be selected large. Since $R_{dj} \gg R_{\mathrm{line}}$, the above expression can be written as

$$\frac{i_{\mathrm{dc}1}}{i_{\mathrm{dc}2}} = \frac{R_{d2} + R_{\mathrm{line}2}}{R_{d1} + R_{\mathrm{line}1}} \approx \frac{R_{d2}}{R_{d1}}. \tag{4}$$

But the abovementioned assumption is suitable for large R_{dj}. For small R_{dj}, precise current sharing cannot be ensured. Meanwhile, voltage regulation cannot be ensured with large virtual resistance. This is graphically shown in Figure 5.

2.2.2. Output Voltage Deviation. Node voltage deviation can be written as

$$\Delta v_j = v_s - v_{sj} = i_{\mathrm{dc}j} R_{dj} \quad \text{where } j = 1, 2. \tag{5}$$

Figure 6 shows the voltage deviation with different virtual resistances. Voltage deviation is of zero value when the sources operate in an open circuit mode (source currents are zero) as shown in Figure 6. When the current by the sources is not zero, voltage deviation appears, and its value varies with the variation in load. To limit the output voltage deviation within acceptable levels, the droop coefficient R_{dj} should be limited as

$$R_{dj} \leq \frac{\Delta v_{\max}}{i_{\mathrm{fl}j}}, \tag{6}$$

where $i_{\mathrm{fl}j}$ is full-load current of source-j.

2.3. Distributive Control. Disadvantages associated with the decentralized (droop control) and centralized control can be adjusted using distributed control which is an alternative solution to achieve efficient load sharing. As a substitute of

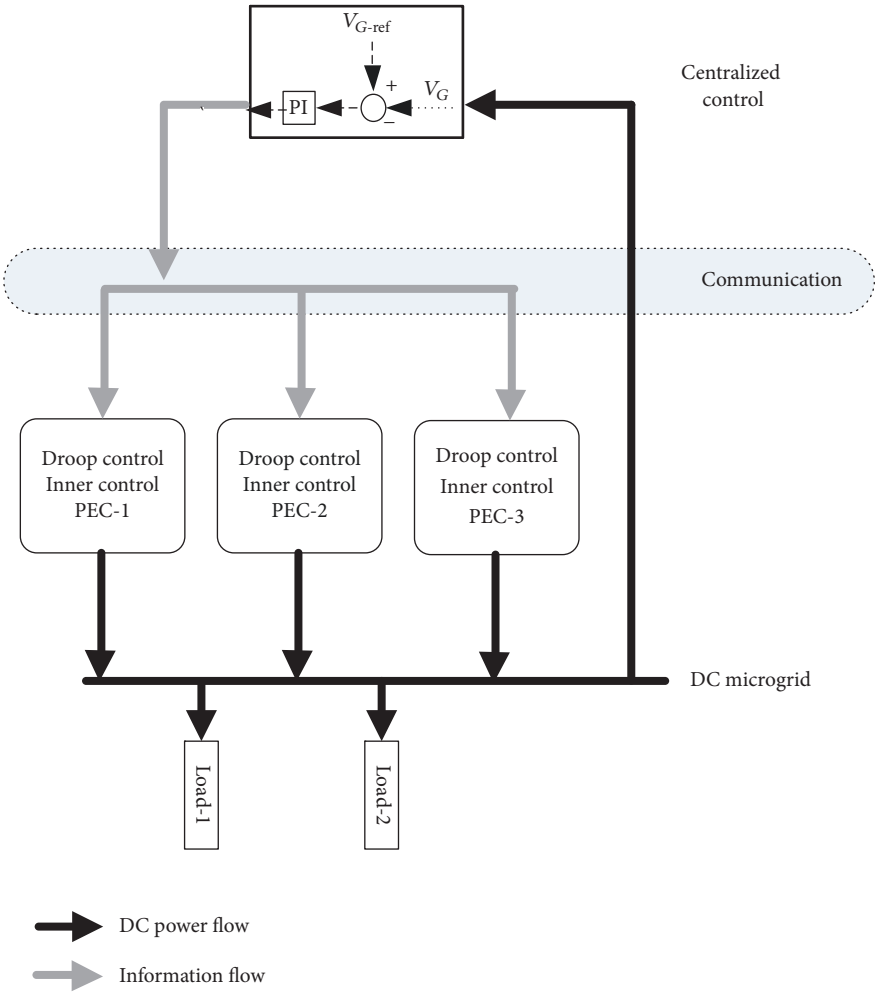

Figure 2: Centralized control in a DC microgrid.

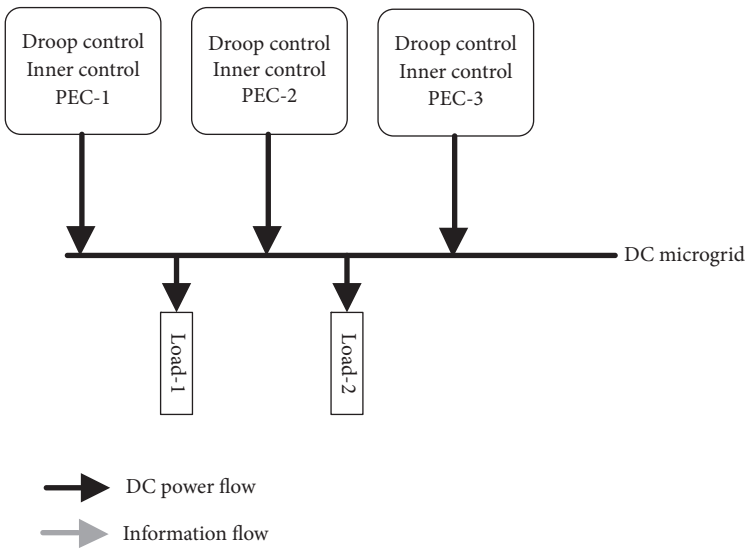

Figure 3: Decentralized control.

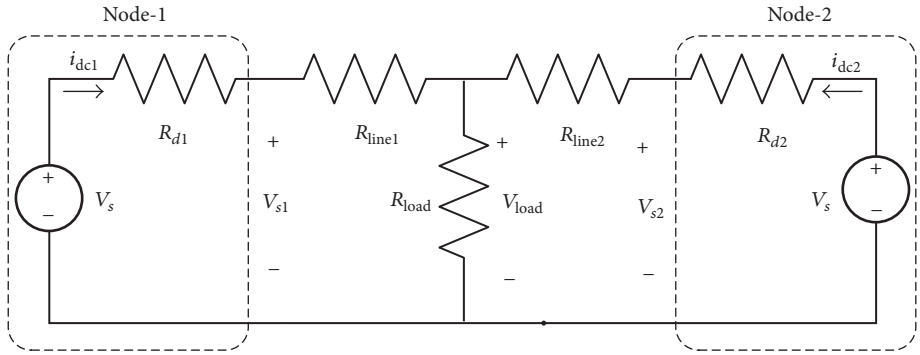

Figure 4: Thevenin equivalent circuit of a DC microgrid with two sources sharing the same load.

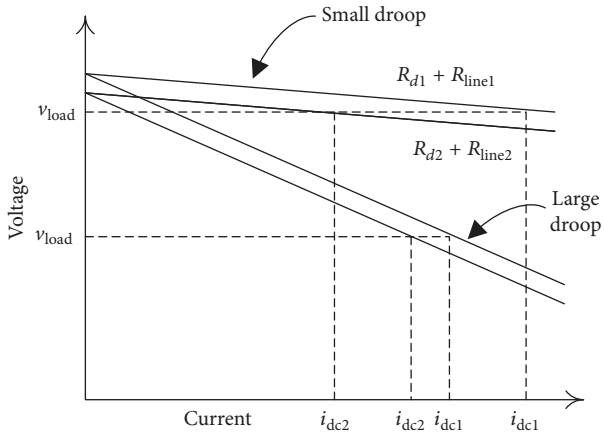

Figure 5: Current sharing inaccuracy using droop control [7].

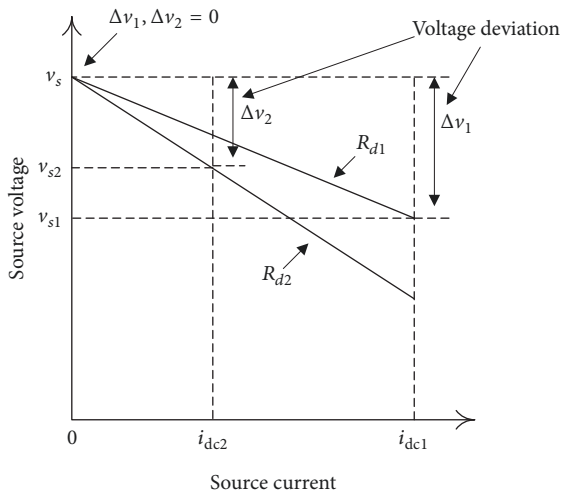

Figure 6: Voltage deviation with a variation in droop resistances [8].

the single central controller, distributive control is distributed among every PE converter. In [24], DC bus signaling (DBS) is proposed for distributed control in which DC voltage is used to communicate the decision about the converters' operation. In DBS, every entity in the system senses the DC voltage level for operation and decisions, which limits the sources, loads, and storage because DC bus voltage cannot be allocated unlimitedly. Furthermore, some extreme situations (e.g., overvoltage/current and fully charged/undercharged battery) are not addressed in DBS. In [41], a current sharing line is proposed and distributed, in which the average current is communicated among converters for operation. In DC microgrids, sources are displaced from each other over a region. Thus, the current sharing bus needs to be distributed over the region with the power lines. This may inject substantial noise which can degrade the system performance. In [42], a distributive secondary control using power line signaling (PLS) is presented. The major problem in PLS is that it is has slow communication. Further, electromagnetic compatibility issues need to be addressed when using it with electronic devices.

In this paper, a distributive control for DC microgrids using low bandwidth communication is proposed and is shown in Figure 7.

To determine the value of current to be shared by each source, the controller of each source communicates among the other sources and informs about the per-unit (p.u.) current supplied by it. This information is used by each controller to determine the total current supplied by all sources, which is given as

$$i_T^{\text{pu}} = \sum_{m=1}^{n} i_j^{\text{pu}}, \tag{7}$$

where i_j^{pu} is the p.u. current of source-j and n is the number of sources. The reference current of each source i_j^{ref} is calculated as

$$i_j^{\text{ref}} = k_j i_j^{\text{rated}} i_T^{\text{pu}}, \tag{8}$$

where k_j and i_j^{rated} are the load sharing factor and rated current of source-j, respectively.

In the architecture shown in Figure 7, the p.u. current of each source is shared. Hence, the data transmitted over the communication link by each source is 2 bytes and the total data transmitted is $2n$ bytes. Data read by each source is $2(n-1)$ bytes. Hence, the technique used for communication has to manage small data, and thus a low bandwidth communication is feasible. So, computer area network (CAN) based communication is used for DC microgrids in this paper.

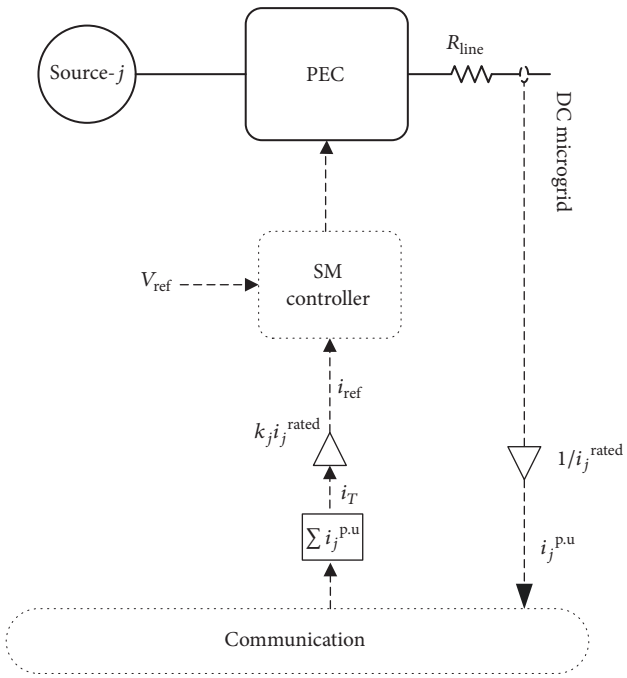

Figure 7: Distributive control architecture.

2.3.1. Sliding Mode Control. Each source in a DC microgrid consists of a PE converter. Linear controllers (PI, PID, and lead-lag) are being used to control the PE converters for the load sharing problem in DC microgrids [30–32]. These controllers require a linearized model of the system, which makes it difficult for them to show good power sharing performance and stability in all operating conditions [33–35]. So, an SM controller is alternatively proposed in [36–40, 43] which ensures stability in all operating conditions. Hence, in this paper, an SM controller technique is proposed for proportional load sharing and stability of DC microgrids.

(1) Modeling. A generalized DC microgrid architecture is shown in Figure 1. An equivalent model of one source with DC microgrid through DC-to-DC PE converter is shown in Figure 8. The source is modeled as voltage source v_s with current i_s, whereas the DC bus of the microgrid is modeled through capacitor C and its associated connecting line current i_{dc}. The source and DC microgrid are interfaced through the DC-to-DC PE converter. The differential equations describing the system dynamics of this model are expressed as follows:

$$\frac{di}{dt} = \frac{-v_{\text{dc}} + uv_s}{L}, \tag{9}$$

where $v_{\text{dc}} = v_{\text{line}} + v_G$, and

$$\frac{dv_{\text{dc}}}{dt} = \frac{i - i_{\text{dc}}}{C}, \tag{10}$$

where i, v_{dc}, v_{line}, v_G, i_{dc}, L, and C are inductor current, bus voltage (capacitor voltage), connecting line voltage, grid voltage, line current, inductance, and capacitance, respectively, whereas u defines the switching state of the MOSFET switch which can be expressed as

$$u = \begin{cases} 1 & \text{switch is “ON”} \\ 0 & \text{switch is “OFF”}. \end{cases} \tag{11}$$

(2) Sliding Mode Controller Analysis. In sliding mode, most of the controllers include error of one or multiple states of the system in the sliding surface (e.g., inductor current or capacitor voltage) [44, 45]. Furthermore, some controllers include error and both of the time derivative and the integral of the error in the sliding surface to stabilize the system [38]. In this case, the sliding surface can be represented as a second-order differential equation for which extensive mathematical analysis is required to guarantee system stability. Another surface is defined in [46] for the improvement in the steady-state error and settling time, which includes voltage error and square of the capacitor current of the system.

This paper proposes an SM controller which is designed to achieve both proportional power sharing and dynamic stability of DC microgrids. The sliding surface is selected to ensure load sharing and precise voltage regulation. Thus, it is formed using the bus voltage error, current error, and integral of the bus voltage error. This way, the SM controller can detect and minimize the voltage and current errors. Further, the integral action is included to reduce the steady-state voltage error. The proposed sliding surface Ψ is given in

$$\Psi = \alpha e_v + \beta e_i + \int e_v \, dt, \tag{12}$$

where

$$\begin{aligned} e_v &= v_{\text{dc}} - v_{\text{dc}}^{\text{ref}}, \\ e_i &= i - i^{\text{ref}}, \end{aligned} \tag{13}$$

whereas e_v, e_i, $v_{\text{dc}}^{\text{ref}}$, and i^{ref} are voltage error, current error, reference bus voltage, and reference inductor current, respectively, while α and β are parameters of the sliding surface. Figure 9 shows the block diagram of the SM control system.

The derivative of the sliding surface is used to ensure the existence of SM which is given as

$$\frac{d\Psi}{dt} = \alpha \frac{dv_{\text{dc}}}{dt} + \beta \frac{di}{dt} + e_v. \tag{14}$$

Substituting (9) and (10) into (14) leads to

$$\frac{d\Psi}{dt} = \frac{\alpha}{C}\left(i - i_{\text{dc}}\right) - \frac{\beta}{L}\left(v_{\text{dc}} - uv_s\right) + e_v. \tag{15}$$

For the existence of SM, the conditions described in (16) need to be fulfilled [47], which ensures that, in steady-state condition, $v_{\text{dc}} = v_{\text{dc}}^{\text{ref}}$ and $i = i^{\text{ref}}$. Hence, voltage and current achieve the desired reference.

$$\begin{aligned} \Psi &= 0, \\ \frac{d\Psi}{dt} &= 0. \end{aligned} \tag{16}$$

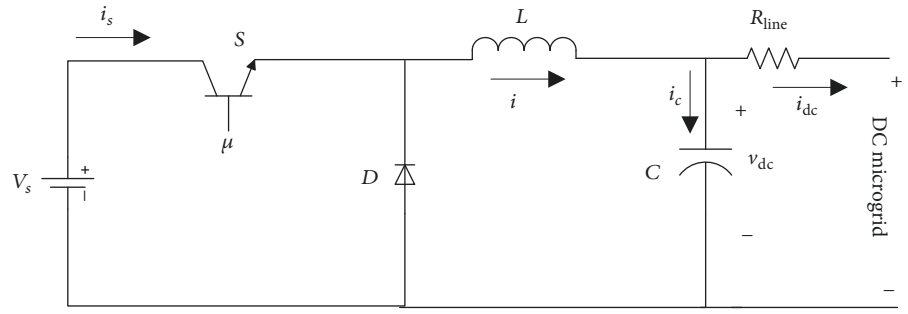

Figure 8: Equivalent model of one source with a DC microgrid.

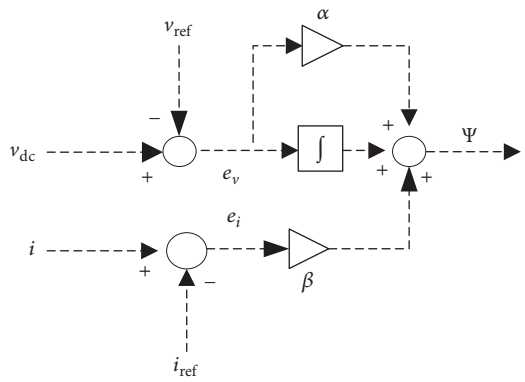

Figure 9: Block diagram of the SM controller.

To ensure the existence of SM (i.e., guaranteeing (16)), the transversality, reachability, and equivalent control conditions must be guaranteed.

(i) Transversality Condition. The transversality condition describes the system controllability. Thus, this condition must be satisfied to allow the system dynamics to be affected by the SM controller [47]. It ensures that the control variable is present in the derivative of sliding surface. It can be expressed as

$$\frac{d}{du}\left(\frac{d\Psi}{dt}\right) \neq 0. \tag{17}$$

Substituting (15) into (17) results in

$$\frac{d}{du}\left(\frac{d\Psi}{dt}\right) = \frac{\beta}{L}\left(v_s\right) \neq 0. \tag{18}$$

Equation (18) depends on the value of β. Section 3.3 determines that the value of β must be positive to guarantee a stable system behavior. Moreover, v_s and L are positive quantities. Hence, (17) will be fulfilled and the transversality condition of the system is satisfied.

(ii) Reachability Condition. The reachability condition describes the system's ability to reach the sliding surface [47, 48]. Thus, the reachability condition ensures that the system will always be directed towards the sliding manifold. Mathematically, it is described in

$$\begin{aligned} \lim_{\Psi\to 0^-} \left.\frac{d\Psi}{dt}\right|_{u=1} &> 0, \\ \lim_{\Psi\to 0^+} \left.\frac{d\Psi}{dt}\right|_{u=0} &< 0. \end{aligned} \tag{19}$$

Substituting (15) into (19), it can be expressed as

$$\begin{aligned} \frac{\alpha}{C}\left(i - i_{\text{dc}}\right) + \frac{\beta}{L}\left(v_s - v_{\text{dc}}\right) + e_v &> 0 \\ -\frac{\alpha}{C}\left(i_{\text{dc}} - i\right) - \frac{\beta}{L}v_{\text{dc}} + e_v &< 0. \end{aligned} \tag{20}$$

The conditions in (20) must be fulfilled to guarantee that the SM will exist, and the system will be derived to the desired operating condition.

(iii) Equivalent Control Condition. The equivalent control condition defines the local stability of the system and enables that system to remain trapped inside the sliding surface [47, 48]. Mathematically, the equivalent control condition can be expressed as in

$$\begin{aligned} \left.\frac{d\Psi}{dt}\right|_{u=u_{\text{eq}}} &= 0 \longrightarrow \\ 0 < u_{\text{eq}} &< 1. \end{aligned} \tag{21}$$

Substituting $u = u_{eq}$ in (15) and equating to zero result in the following expression:

$$u_{eq} = \frac{v_{dc}}{v_s} - \frac{\alpha}{\beta}\left(\frac{L}{C}\right)\left(\frac{i - i_{dc}}{v_s}\right) - \frac{L}{\beta v_s} e_v. \tag{22}$$

Fulfilling the reachability condition also verifies the equivalent control condition.

(3) Sliding Mode Dynamics. The inequalities in (20) generally describe the existence of SM. These inequalities do not give information about the selection of the sliding parameters α and β. This section deals with the selection of sliding parameters based on the desired dynamic behavior. Thus, the stability of the system is fulfilled. For this purpose, closed loop dynamics in time domain of the system are achieved by putting sliding surface $\Psi = 0$ in (12). The dynamics are given in

$$e_i = \frac{\alpha}{\beta} e_v + \frac{1}{\beta}\int e_v \, dt. \tag{23}$$

The closed loop dynamics in Laplace domain are given in

$$\frac{e_i(s)}{e_v(s)} = \frac{1 + \alpha s}{\beta s}. \tag{24}$$

Formerly, the voltage dynamics of the DC bus defined in (10) are imposed by (24). Further, to find complete closed loop dynamics of the system, (10) can be expressed in Laplace domain as

$$Cs v_{dc}(s) = i(s) + i_{dc}(s). \tag{25}$$

Finally, combining (24) and (25), the complete closed loop dynamics of the DC bus voltage can be expressed as

$$\begin{aligned} v_{dc}(s) = &-\frac{\beta s}{C\beta s^2 + \alpha s + 1} i_{dc}(s) \\ &+ \frac{1 + \alpha s}{C\beta s^2 + \alpha s + 1} v_{dc}^{ref}(s) \\ &+ \frac{\beta s}{C\beta s^2 + \alpha s + 1} i^{ref}(s). \end{aligned} \tag{26}$$

It is shown in (26) that closed loop dynamics depend on the perturbation introduced by the DC bus current and the reference. Since the reference is a constant value and the DC bus current depends on the source and load power requirements, (26) can be expressed as (27) which is used to design sliding parameters α and β of the SM controller.

$$\frac{v_{dc}(s)}{i_{dc}(s)} = -\frac{s}{Cs^2 + (\alpha/\beta)s + 1/\beta}. \tag{27}$$

Finally, it is established in (27) that both sliding parameters α and β must have a positive value to ensure stable SM dynamics; otherwise, the system will show an unstable behavior.

(4) Design of Sliding Mode Dynamic Behavior. The dynamics shown in (27) demonstrate that the SM controller will compensate any perturbation produced in the bus current i_{dc} (i.e., $\lim_{\Psi\to\infty}(v_{dc}(s)/i_{dc}(s)) = 0$). However, large undershoots and overshoots in bus voltage can turn off or destroy the load. Therefore, the dynamics of the bus voltage should be controlled. The characteristic polynomial in the denominator of (27) shows that it is a second-order system of the form given in

$$s^2 + 2\zeta\omega_0 s + \omega_0^2 = 0, \tag{28}$$

where ζ and ω_0 are the damping ratio and undamped natural frequency, respectively. Comparing (28) with the denominator of (27), ζ and ω_0 can be calculated as

$$\begin{aligned} \omega_0 &= \sqrt{\frac{1}{\beta C}} \\ \zeta &= \frac{\alpha}{2}\sqrt{\frac{1}{\beta C}}. \end{aligned} \tag{29}$$

ζ and ω_0 can control the response of the system. Two types of responses are considered in this paper: underdamped and critically damped response. The characteristics of these are discussed below.

(i) Underdamped Response. In this type, the controller enables the system response to reach the desired voltage faster. But this faster response is achieved at the expense of oscillation around the desired voltage. The loads that are sensitive to the voltage drops but not sensitive to the oscillations are suitable to be controlled using underdamped response (e.g., microprocessors) [49].

(ii) Critically Damped Response. In this type, the controller enables the system response to avoid oscillations. But the response will experience a longer delay reaching the desired voltage level. The loads that are sensitive to the oscillation but show tolerance to the voltage drops are suitable to be controlled through critically damped response (e.g., variable frequency drive motors) [50].

An overdamped response is not considered in this paper because it does not achieve any improvement over the critically damped response.

(a) Underdamped Response. The underdamped time domain response of the system presented in (27) is given in (30) for the values of α and β that will lead to the underdamped response. The condition to guarantee the underdamped response is given in (31). Hence,

$$\begin{aligned} v_{dc}(t) = &\frac{-\Delta i_{dc}}{C\left(\sqrt{(\alpha/2\beta C)^2 - (1/\beta C)}\right)} e^{((\alpha/2\beta C)t)} \\ &\cdot \sin\left(\sqrt{\left(\frac{\alpha}{2\beta C}\right)^2 - \left(\frac{1}{\beta C}\right)}\right) \end{aligned} \tag{30}$$

$$\frac{\alpha^2}{4C} < \beta, \tag{31}$$

where Δi_{dc} represents the step change in the DC bus current. Percentage overshoot for underdamped response is given in

$$\%\ \mathrm{OS} = 100e^{(-\zeta\pi/\sqrt{1-\zeta^2})}. \tag{32}$$

Conversely, the damping ratio ζ for a specific percentage overshoot is given in

$$\zeta = \sqrt{\frac{\ln(\%\ \mathrm{OS}/100)}{\pi^2 + (\ln(\%\ \mathrm{OS}/100))^2}}. \tag{33}$$

The settling time of the underdamped response is given in

$$T_s = \frac{\ln(\text{tolerance fraction})}{\zeta\omega_0}. \tag{34}$$

Equations (32) to (34) can be used to design the SM controller for specific design parameters. Finally, the constraints in (20) must be satisfied for the existence of the SM. Moreover, the selected values of α and β must satisfy the constraint in (31) which is the condition for underdamped response.

(b) Critically Damped Response. Critically damped time domain response is given in (35) while ensuring that the values of α and β will lead to the critically damped response. The condition for this response is given in (36). Hence,

$$v_{dc}(t) = \frac{-\Delta i_{dc}}{C}(t)\, e^{((\alpha/2\beta C)t)} \tag{35}$$

$$\beta = \frac{\alpha^2}{4C}. \tag{36}$$

Finally, the constraints defined in (20) must be satisfied for the existence of SM. Further, (36) must be satisfied for the critically damped response.

(5) Sliding Mode Hysteresis Control. In an ideal situation, the SM controller will switch the DC-to-DC converter at infinite frequency with system trajectories moving along the sliding surface when the system enters the SM operation. This condition is shown in Figure 10(a). However, the practical switch of the DC-to-DC converter will experience some switching imperfections and time delays. This will produce a dynamic behavior in the locality of the sliding surface which is identified as chattering as shown in Figure 10(b) [47, 48].

If the chattering produced in the sliding surface is left uncontrolled, the converter will start self-oscillating at a high frequency. This behavior of the converter is not desirable due to the high switching losses. Further, the exact switching frequency in the produced chattering cannot be predicted. Therefore, the converter design and component selection will turn out to be difficult. To solve these issues, the control law u is redefined as

$$u = \begin{cases} 0 = \text{“OFF”} & \text{when } \Psi > k \\ 1 = \text{“ON”} & \text{when } \Psi < -k \\ \text{unchanged} & \text{otherwise,} \end{cases} \tag{37}$$

where k is a positive number. Usually in SMC, a hysteresis band is introduced to tackle the chattering problem. With this alteration, the converter switch will turn on when $\Psi < -k$ and turn off when $\Psi > k$. In the region $-k \le \Psi \le k$, the converter switch remains unchanged and maintains its former state. Therefore, introducing a region $-k \le \Psi \le k$ in which no switching occurs, the switching frequency can be controlled by varying the magnitude of k.

Table 1: DC-to-DC converter parameters.

Parameters	Value
Desired voltage	48 V
Switching frequency	10 kHz
Inductor, L	100 μH
Capacitor, C	4000 μF

Table 2: Node parameters of DC microgrid.

Parameters	Node-1	Node-2
Desired voltage	48 V	
Source rated power	250 W	500 W
Load resistance	6	
Voltage and current regulation required	≤±5%	

Table 3: Connecting cable parameters of DC microgrid.

Parameters	Branch-12	Branch-23
Current rating	20 A	
Cable resistance	205 mΩ	2 mΩ

3. Results and Discussion

To examine the load sharing performance among parallel connected sources, a DC microgrid with two sources connected in a parallel configuration to the load through connecting lines is proposed and shown in Figure 11. This type of configuration can be easily extendable for more sources and microgrids in parallel configuration. This type of system is attractive for remote areas where the national grid cannot be easily extendable due to the high cost associated with the installation of new transmission lines. Thus, a two-source DC microgrid system for load sharing is simulated using MATLAB/Simulink. Each source consists of a DC-to-DC converter. The parameters of the DC-to-DC converter are selected to support maximum voltage and current levels equal to 50 V and 10 A, respectively. Therefore, the converter supports a maximum power of 500 W. The parameters for the DC-to-DC converter are given in Table 1.

3.1. Results Using Droop Control. The details of nodes and connecting lines are given in Tables 2 and 3, respectively. Each source using droop control is shown in Figure 12.

A two-source DC microgrid shown in Figure 11 is simulated using droop control. To observe the steady-state behavior, assume that the load is drawing rated current and

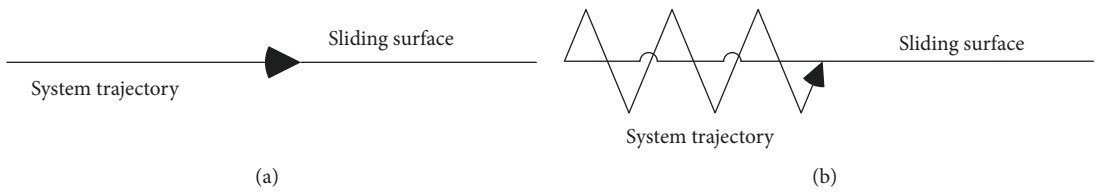

Figure 10: System trajectory with (a) ideal SM and (b) practical SM.

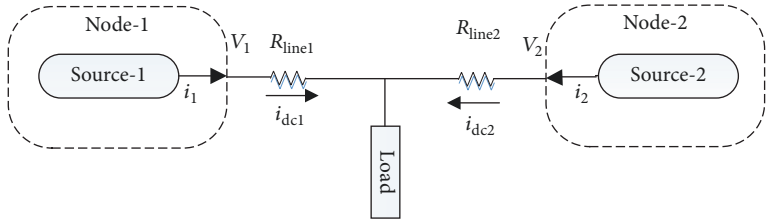

Figure 11: A two-source DC microgrid.

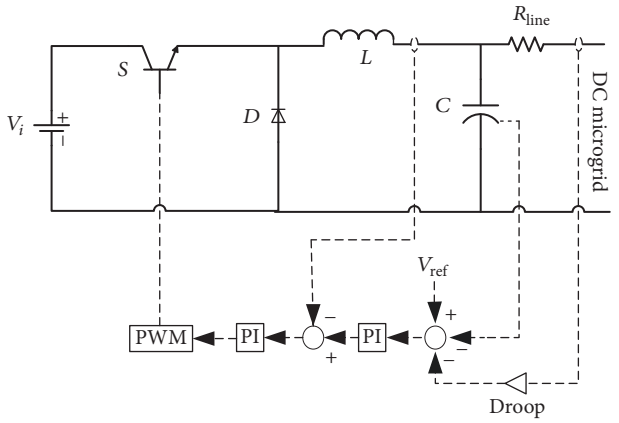

Figure 12: DC-to-DC buck converter using droop control.

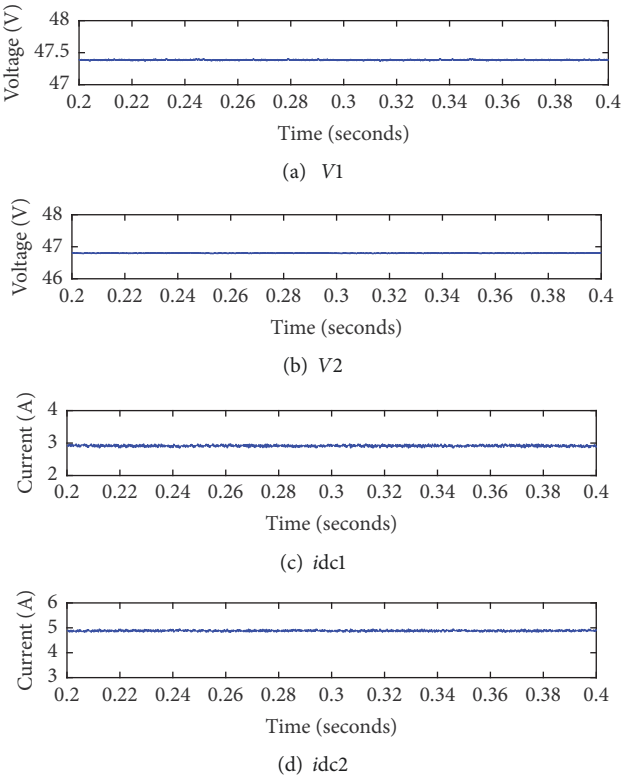

Figure 13: Node voltages and source currents with droop gain 0.2 Ω.

the steady state is reached. For equal load sharing, source-1 and source-2 are simulated for the same power rating. Thus, droop gains $R_{d1} = R_{d2} = 0.2\,\Omega$ are selected for equal load sharing. Node voltage and current by each source are shown in Figure 13.

For droop gain 0.2 Ω, the steady-state current supplied by source-1 and source-2 is 2.9 and 4.9 A, respectively, as shown in Figure 13. For equal load sharing, the desired current to be supplied by each source is 4 A. The maximum deviation observed in the supplied current is 27.5%. Steady-state node voltages at source-1 and source-2 are 47.4 and 46.8 V, respectively. The deviation observed in node voltages at no load and full load is 2.5%. These results show that small droop gains ensure decent voltage regulation, but the load sharing performance is not acceptable. For a large droop gain of 1.9 Ω, the current supplied by source-1 and source-2 is 3.8 and 4.2 A, respectively. The observed deviation in the supplied currents is 5%, which is acceptable and lower than in the earlier case. But the deviation in node voltages has increased to 16% which cannot be acceptable for the loads.

3.2. Results Using Sliding Mode Control. Figure 14 shows each source with distributed control using the SM controller. The p.u. value of each source current is communicated to the other sources every 10 ms. The total communication delay is around 0.1 ms.

To observe the steady-state behavior with distributed architecture using SM controller, the two-source DC microgrid shown in Figure 11 is simulated and the results are shown in Figure 15. The current supplied by source-1 and source-2 is

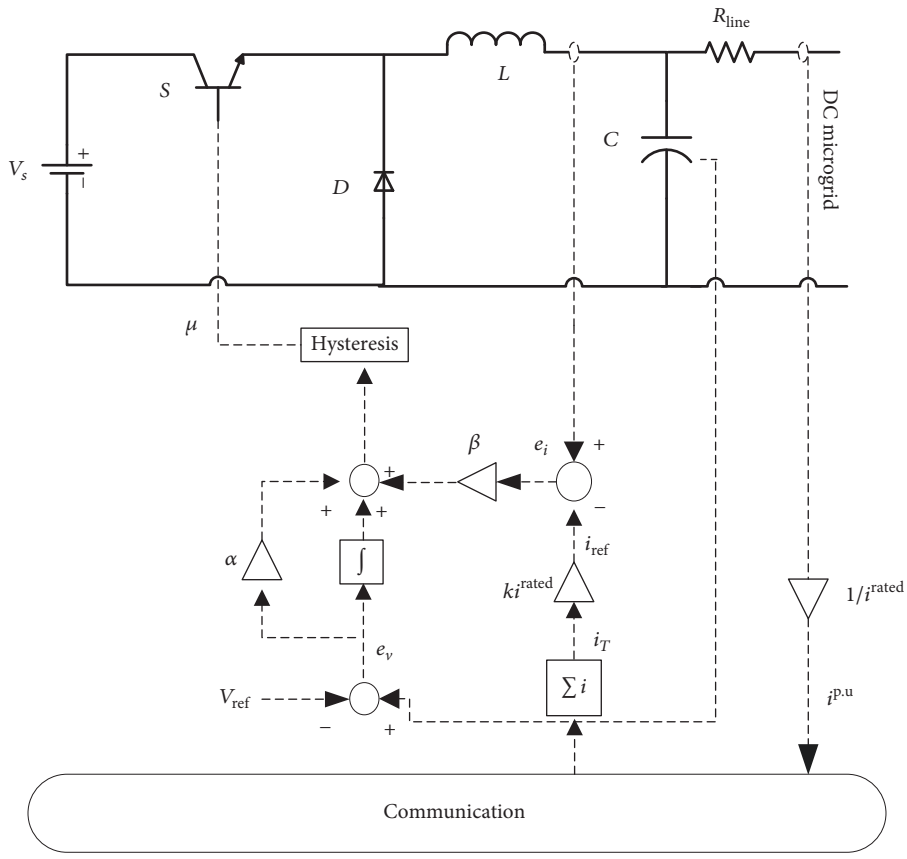

Figure 14: DC-to-DC buck converter with a distributed architecture using SM controller.

3.91 and 3.92 A, respectively. The observed deviation in the supplied currents is 2.08% which is a significantly low value compared to the droop controlled DC microgrid. Further, the node voltages at source-1 and source-2 are 47.78 and 47 V, respectively. The deviation observed in the node voltages is 2.25%. This confirms the steady-state load sharing and voltage regulation performance of the proposed distributed SM controller.

Further, Figure 16 shows that source-1 is sharing 25% and source-2 is sharing 75% of the rated load current. The current deviation observed is 4.1% which shows the effectiveness of the proposed architecture using the SM controller. In addition, simulations are carried out to see the effect of connecting line resistance and the results are summarized in Table 4. Each column represents the fixed value of connecting line resistance of source-1, R_{line1}, and each row represents the fixed value of connecting line resistance of source-2, R_{line2}. Each entity in Table 4 represents voltage and current sharing deviation. It can be observed that connecting line resistance affects the load sharing between sources.

To observe the transient condition, a step load of 3 Ω is applied at 0.5 s when the system is operating in steady state at the rated load, as shown in Figure 17. At the instant when a step change in load is applied, node voltages drop shortly as shown in Figure 17. However, within 25 ms, node voltages of source-1 and source-2 settle down to 49.29 and 46.83 V, respectively. This corresponds to a voltage deviation of 2.68%. The currents supplied are 11.96 and 11.45 A. The deviation in the supplied currents is 4.5%.

Furthermore, the dynamic behavior of node voltage is investigated for underdamped and critically damped responses. The sliding parameters α and β are selected positive according to the conditions defined in (31) and (36). The values of α and β are listed in Table 5. Figure 18 shows node voltage when the load resistance is changed from 6 to 3 Ω at 0.5 s with sliding parameters that show underdamped and critically damped responses. The results of settling time are summarized in Table 5. It can be observed that as the value of ζ is increased from 0.1 to 0.6, the underdamped response is improved with smaller settling time. This response is in good agreement with the presented theory. Additionally, for $\zeta = 1$, the response is critically damped with further improved settling time as presented in theory. These results show the good dynamic performance of the SM controller with distributed architecture.

3.3. Fail-Safe Performance of Distributed Control Architecture. A significant improvement in the distributed architecture is that it provides high reliability. To prove this claim, a three-source DC microgrid shown in Figure 19 is simulated for fault condition and shown in Figure 20. The parameters of each source are the same as given in Table 1. Source-1 and source-2 are connected to the load through connecting line resistances. But source-3 is directly connected to the load. At steady state,

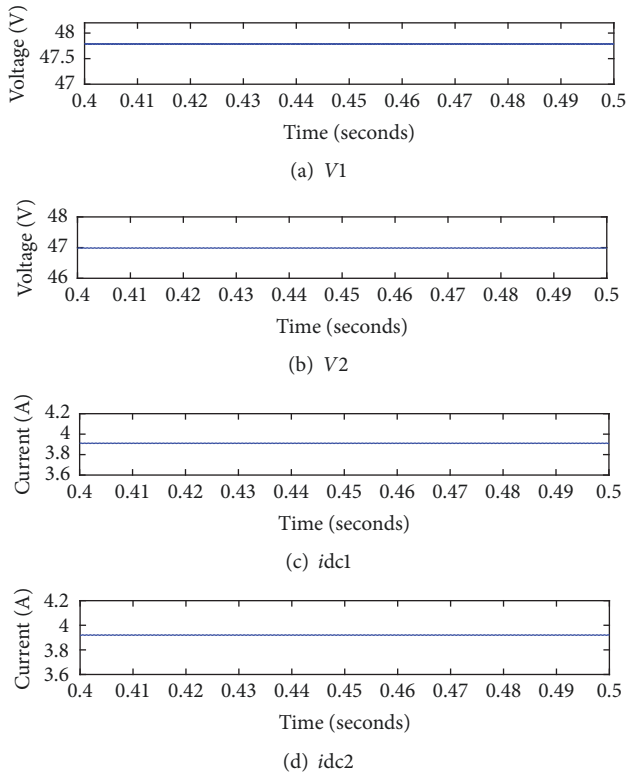

Figure 15: Node voltages and source currents with a distributed architecture using SM controller.

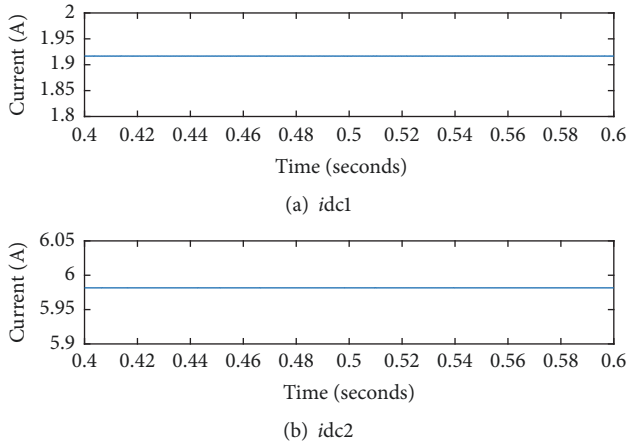

Figure 16: Source 1 with 25% and source 2 with 75% load sharing of the rated load.

the voltage across the load is 47.04 V. The three sources supply 3.915, 3.91, and 3.93 A. The maximum deviation observed in the supplied currents is 2.25%.

If one source becomes faulty, the capacity of the other two sources is enough to satisfy the load. Failure of source-2 is simulated by removing its power supply at 0.5 s. Under this fault, the voltage across loads and the supplied currents by sources are shown in Figure 20. After this fault, the system reaches the steady state in about 25 ms. The voltage across loads is maintained at 47.35 V. The supplied current

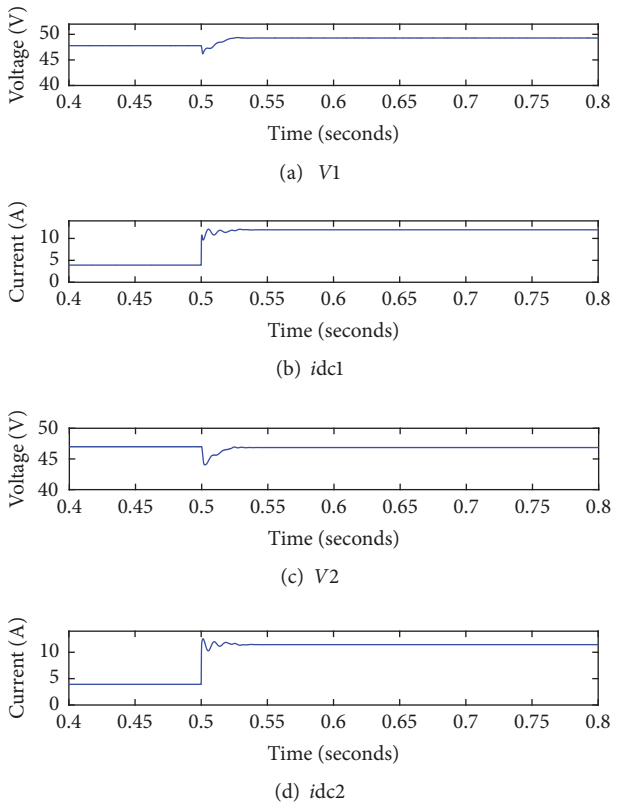

Figure 17: Transient response when a step load of 3 Ω is applied at 0.5 seconds.

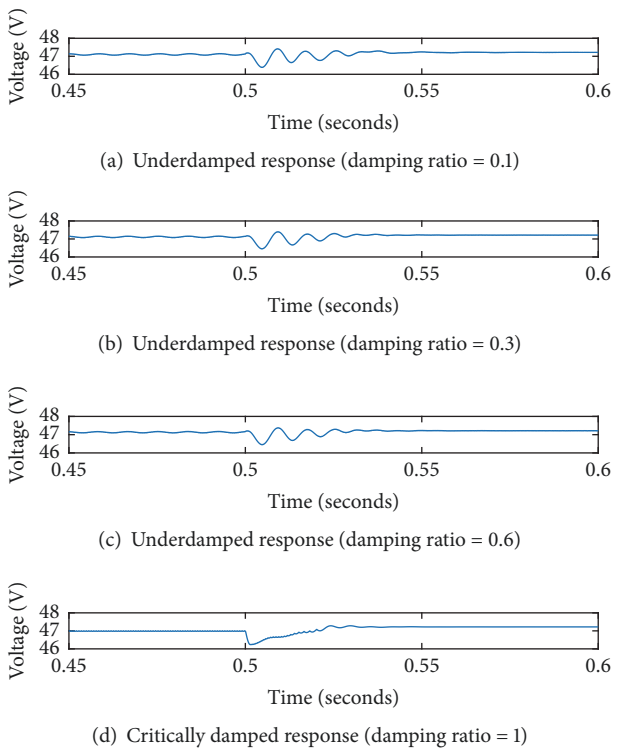

Figure 18: Voltage response of a source when load resistance is changed from 6 to 3 Ω at 0.5 seconds.

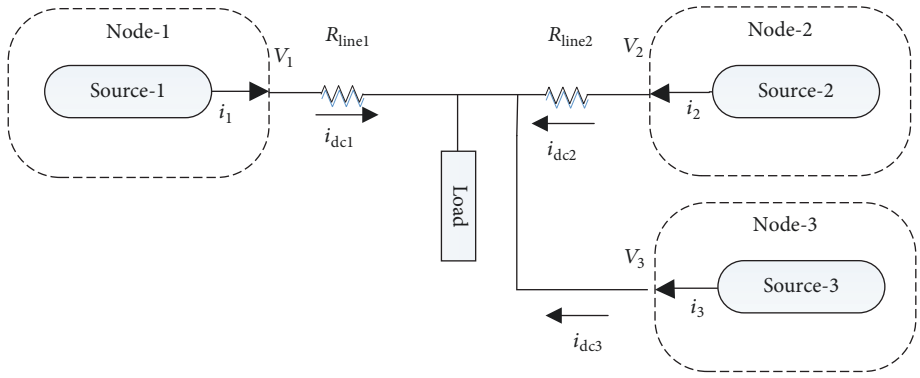

Figure 19: A three-source DC microgrid.

Table 4: Connecting cable parameters of DC microgrid.

	$R_{line1} = 0.5 \times 205\,m\Omega$	$R_{line1} = 1 \times 205\,m\Omega$	$R_{line1} = 2 \times 205\,m\Omega$
$R_{line2} = 0.5 \times 2\,m\Omega$	1.92% V/V, 1.9% A/A	2.05% V/V, 2.24% A/A	2.26% V/V, 2.52% A/A
$R_{line2} = 1 \times 2\,m\Omega$	1.95% V/V, 1.925% A/A	2.08% V/V, 2.25% A/A	2.27% V/V, 1.875% A/A
$R_{line2} = 2 \times 2\,m\Omega$	1.99% V/V, 1.95% A/A	2.12% V/V, 2.75% A/A	2.27% V/V, 1.925% A/A

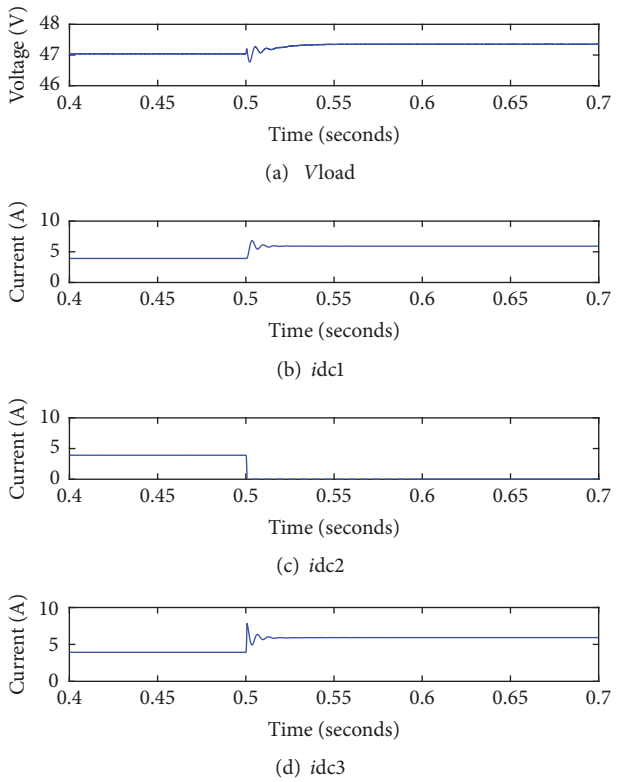

Figure 20: Transient response during fault on source-2 at 0.5 seconds.

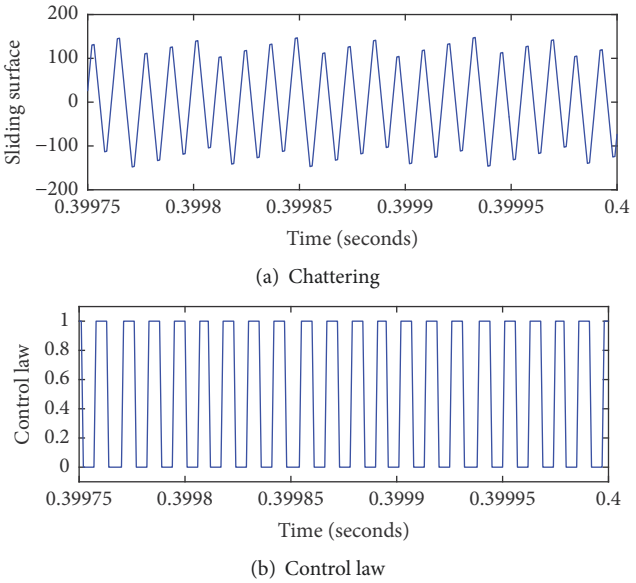

Figure 21: Sliding surface with chattering and control law.

by source-1 and source-3 is 5.91 and 5.93 A, respectively. This corresponds to 1.5% deviation in the supplied current. This confirms the performance of the distributed architecture using SM controller during source failure. To show the effect of chattering produced, the sliding surface of a source is simulated and shown in Figure 21. Figure 21(a) shows the produced chattering which is controlled using a hysteresis band as defined in (37). The value of k is selected as 100 based on the criteria reported in [51]. Figure 21(b) shows the control signal which is used to operate the converter switch.

3.4. Problems in Distributive Sliding Mode Application. The delays in the communication channel will directly affect the transient behavior of the system, while the steady-state response is not affected by the communication delays. Further, the SM controller is realized through analog integrated circuits. The following are some design issues in analog implementation.

Table 5: Voltage dynamic behavior for different values of ζ.

Damping ratio ζ	Sliding parameter (α, β)	Settling time	Response type
$\zeta = 0.1$	(0.28, 100)	0.05 s (50 ms)	Underdamped
$\zeta = 0.3$	(0.85, 100)	0.04 s (40 ms)	Underdamped
$\zeta = 0.6$	(1.7, 100)	0.03 s (30 ms)	Underdamped
$\zeta = 1$	(2.85, 100)	0.02 s (20 ms)	Critically damped

(i) Selecting the variables is a serious concern because selecting more variables results in more computations and sensing required which will increase the complexity of the system.

(ii) Selecting the integral and derivative of the variables involves noise sensitivity. These variables are desired to be indirectly controlled; for example, dV_c/dt can be achieved through sensing capacitor current.

(iii) The produced chattering is a big challenge in SM. It produces excessive switching losses and limits the selection of the switching device.

(iv) Restrictions of the analog components (e.g., slew rate, bandwidth, and saturation limits) need to be carefully considered for the proper control operation.

4. Conclusion

A distributed architecture using an SM controller is proposed for proportional load sharing and stability of DC microgrids. DC microgrids are a reliable method to provide efficient power to the consumer in the presence of renewable sources. Droop controllers which are local controllers can achieve good load sharing at the cost of voltage regulation. Further, voltages at different nodes of the DC microgrid are not the same. So, it is difficult to achieve load sharing when the connecting line resistances among the sources are considerable. A centralized controller can achieve these objectives using a high speed communication link. However, it loses reliability due to the single point failure. Additionally, these controllers are realized through proportional integral (PI) controllers which cannot ensure load sharing and stability in all operating conditions. To address limitations, a distributed architecture using an SM controller utilizing low bandwidth communication is proposed for DC microgrids in this paper. A system model is developed and its transversality, reachability, and equivalent control condition are verified. Furthermore, the dynamic behavior of the modeled system is investigated for underdamped and critically damped responses. Detailed simulation results showed good performance of the proposed controller.

Conflicts of Interest

The authors declare that there are no conflicts of interest regarding the publication of this paper.

References

[1] K.-T. Mok, M.-H. Wang, S.-C. Tan, and S. Y. R. Hui, "DC electric springs—a technology for stabilizing DC power distribution systems," *IEEE Transactions on Power Electronics*, vol. 32, no. 2, pp. 1088–1105, 2017.

[2] K. A. Saleh, A. Hooshyar, and E. F. El-Saadany, "Hybrid passive-overcurrent relay for detection of faults in low-voltage DC grids," *IEEE Transactions on Smart Grid*, vol. 8, no. 3, pp. 1129–1138, 2017.

[3] L. Meng, Q. Shafiee, G. Ferrari Trecate et al., "Review on control of DC microgrids," *IEEE Journal of Emerging and Selected Topics in Power Electronics*, vol. 99, 1 page, 2017.

[4] X. Li, L. Guo, S. Zhang et al., "Observer-based DC voltage droop and current feed-forward control of a DC microgrid," *IEEE Transactions on Smart Grid*, vol. 99, 1 page, 2017.

[5] T. V. Vu, S. Paran, F. Diaz-Franco, T. El-Mezyani, and C. S. Edrington, "An alternative distributed control architecture for improvement in the transient response of DC microgrids," *IEEE Transactions on Industrial Electronics*, vol. 64, no. 1, pp. 574–584, 2017.

[6] T. Dragicevic, X. Lu, J. C. Vasquez, and J. M. Guerrero, "DC microgrids—part I: a review of control strategies and stabilization techniques," *IEEE Transactions on Power Electronics*, vol. 31, no. 7, pp. 4876–4891, 2016.

[7] S. Anand, B. G. Fernandes, and J. M. Guerrero, "Distributed control to ensure proportional load sharing and improve voltage regulation in low-voltage DC microgrids," *IEEE Transactions on Power Electronics*, vol. 28, no. 4, pp. 1900–1913, 2013.

[8] M. Rashad, M. Ashraf, A. I. Bhatti, D. M. Minhas, and B. A. Ahmed, "Mathematical modeling and stability analysis of DC microgrid using sm hysteresis controller," *International Journal of Electrical Power & Energy Systems*, vol. 95, pp. 507–522, 2018 (Arabic).

[9] A. Esmaeli, "Stability analysis and control of microgrids by sliding mode control," *International Journal of Electrical Power & Energy Systems*, vol. 78, pp. 22–28, 2016.

[10] P. Wang, X. Lu, X. Yang, W. Wang, and D. Xu, "An improved distributed secondary control method for DC microgrids with enhanced dynamic current sharing performance," *IEEE Transactions on Power Electronics*, vol. 31, no. 9, pp. 6658–6673, 2016.

[11] S. D. Tavakoli, M. Mahdavyfakhr, M. Hamzeh, K. Sheshyekani, and E. Afjei, "A unified control strategy for power sharing and voltage balancing in bipolar DC microgrids," *Sustainable Energy, Grids and Networks*, vol. 11, pp. 58–68, 2017.

[12] S. Peyghami, H. Mokhtari, P. C. Loh, P. Davari, and F. Blaabjerg, "Distributed primary and secondary power sharing in a droop-controlled LVDC microgrid with merged AC and DC characteristics," *IEEE Transactions on Smart Grid*, vol. 99, p. 1, 2016.

[13] S. Peyghami, P. Davari, H. Mokhtari, P. C. Loh, and F. Blaabjerg, "Synchronverter-enabled DC power sharing approach for LVDC microgrids," *IEEE Transactions on Power Electronics*, vol. 32, no. 10, pp. 8089–8099, 2017.

[14] Shivam and R. Dahiya, "Robust decentralized control for effective load sharing and bus voltage regulation of DC microgrid based on optimal droop parameters," *Journal of Renewable and Sustainable Energy*, vol. 9, no. 4, p. 045301, 2017.

[15] Z. Liu, Y. Luo, R. Zhuo, and X. Jin, "Distributed reinforcement learning to coordinate current sharing and voltage restoration for islanded DC microgrid," *Journal of Modern Power Systems and Clean Energy*, pp. 1–11, 2017.

[16] S. Peyghami, H. Mokhtari, and F. Blaabjerg, "Hierarchical power sharing control in DC microgrids," in *Microgrid, Advanced Control Methods and Renewable Energy System Integration*, vol. 3, pp. 63–100, Elsevier, 1 edition, 2016.

[17] C. Jin, P. Wang, J. Xiao, Y. Tang, and F. H. Choo, "Implementation of hierarchical control in DC microgrids," *IEEE Transactions on Industrial Electronics*, vol. 61, no. 8, pp. 4032–4042, 2014.

[18] X. Liu, P. Wang, and P. C. Loh, "A hybrid AC/DC microgrid and its coordination control," *IEEE Transactions on Smart Grid*, vol. 2, no. 2, pp. 278–286, 2011.

[19] J. M. Guerrero, J. C. Vasquez, J. Matas, L. G. de Vicuña, and M. Castilla, "Hierarchical control of droop-controlled AC and DC microgrids: a general approach toward standardization," *IEEE Transactions on Industrial Electronics*, vol. 58, no. 1, pp. 158–172, 2011.

[20] X. Lu, J. M. Guerrero, K. Sun, J. C. Vasquez, R. Teodorescu, and L. Huang, "Hierarchical control of parallel AC-DC converter interfaces for hybrid microgrids," *IEEE Transactions on Smart Grid*, vol. 5, no. 2, pp. 683–692, 2014.

[21] J. He and Y. W. Li, "An enhanced microgrid load demand sharing strategy," *IEEE Transactions on Power Electronics*, vol. 27, no. 9, pp. 3984–3995, 2012.

[22] J. M. Guerrero, M. Chandorkar, T.-L. Lee, and P. C. Loh, "Advanced control architectures for intelligent microgrids—part I: decentralized and hierarchical control," *IEEE Transactions on Industrial Electronics*, vol. 60, no. 4, pp. 1254–1262, 2013.

[23] H. Liang, B. J. Choi, W. Zhuang, and X. Shen, "Stability enhancement of decentralized inverter control through wireless communications in microgrids," *IEEE Transactions on Smart Grid*, vol. 4, no. 1, pp. 321–331, 2013.

[24] J. Schönberger, R. Duke, and S. D. Round, "DC-bus signaling: a distributed control strategy for a hybrid renewable nanogrid," *IEEE Transactions on Industrial Electronics*, vol. 53, no. 5, pp. 1453–1460, 2006.

[25] M. C. Chandorkar, D. M. Divan, and R. Adapa, "Control of parallel connected inverters in standalone AC supply systems," *IEEE Transactions on Industry Applications*, vol. 29, no. 1, pp. 136–143, 1993.

[26] S. V. Iyer, M. N. Belur, and M. C. Chandorkar, "A generalized computational method to determine stability of a multi-inverter microgrid," *IEEE Transactions on Power Electronics*, vol. 25, no. 9, pp. 2420–2432, 2010.

[27] J. M. Guerrero, J. Matas, L. G. De Vicuña, M. Castilla, and J. Miret, "Wireless-control strategy for parallel operation of distributed-generation inverters," *IEEE Transactions on Industrial Electronics*, vol. 53, no. 5, pp. 1461–1470, 2006.

[28] H. J. Avelar, W. A. Parreira, J. B. Vieira Jr., L. C. G. De Freitas, and E. A. A. Coelho, "A state equation model of a single-phase grid-connected inverter using a droop control scheme with extra phase shift control action," *IEEE Transactions on Industrial Electronics*, vol. 59, no. 3, pp. 1527–1537, 2012.

[29] W. Yao, M. Chen, J. Matas, J. M. Guerrero, and Z.-M. Qian, "Design and analysis of the droop control method for parallel inverters considering the impact of the complex impedance on the power sharing," *IEEE Transactions on Industrial Electronics*, vol. 58, no. 2, pp. 576–588, 2011.

[30] P. Karlsson and J. Svensson, "DC bus voltage control for a distributed power system," *IEEE Transactions on Power Electronics*, vol. 18, no. 6, pp. 1405–1412, 2003.

[31] M. Mahmoodi, G. B. Gharehpetian, M. Abedi, and R. Noroozian, "Control systems for independent operation of parallel DG units in DC distribution systems," in *Proceedings of the 1st International Power and Energy Conference, PECon*, pp. 220–224, 28-29 Nov. 2006.

[32] M. Mahmoodi, G. B. Gharehpetian, M. Abedi, and R. Noroozian, "A suitable control strategy for source converters and a Novel Load- Generation Voltage Control scheme for DC voltage determination in DC distribution systems," in *Proceedings of the 1st International Power and Energy Conference, PECon*, pp. 363–367, Malaysia, November 2006.

[33] H.-H. Park and G.-H. Cho, "A DC-DC converter for a fully integrated PID compensator with a single capacitor," *IEEE Transactions on Circuits and Systems II: Express Briefs*, vol. 61, no. 8, pp. 629–633, 2014.

[34] M. M. Peretz and S. Ben-Yaakov, "Time-domain design of digital compensators for PWM DC-DC converters," *IEEE Transactions on Power Electronics*, vol. 27, no. 1, pp. 284–293, 2012.

[35] A. Kwasinski, *A microgrid architecture with multiple-input dc/dc converters: applications, reliability, system operation, and control*, Univ. Illinois Urbana-Champaign, Urbana, Ill, USA, 2007.

[36] S. Singh, D. Fulwani, and V. Kumar, "Robust sliding-mode control of dc/dc boost converter feeding a constant power load," *IET Power Electronics*, vol. 8, no. 7, pp. 1230–1237, 2015.

[37] S. I. Serna-Garcés, D. G. Montoya, and C. A. Ramos-Paja, "Sliding-mode control of a charger/discharger DC/DC converter for DC-bus regulation in renewable power systems," *Energies*, vol. 9, no. 4, article no. 245, 2016.

[38] S. I. Serna-Garcés, R. E. Jiménez, and C. A. Ramos-Paja, "Sliding-mode control of a Dc/Dc postfilter for ripple reduction and efficiency improvement in POL applications," *Journal of Applied Mathematics*, vol. 2013, Article ID 915146, 10 pages, 2013.

[39] N. Vázquez, Y. Azaf, I. Cervantes, E. Vázquez, and C. Hernández, "Maximum power point tracking based on sliding mode control," *International Journal of Photoenergy*, vol. 2015, Article ID 380684, 8 pages, 2015.

[40] J. Cabiles-Magsino, R. C. Guevara, and M. Escoto, "Implementation of sliding mode control for current sharing in fixed frequency voltage regulator modules," in *Proceedings of the IEEE Region 10 Conference: Sustainable Development Through Humanitarian Technology, TENCON 2012*, Philippines, November 2012.

[41] W. Qiu and Z. Liang, "Practical design considerations of current sharing control for parallel VRM applications," in *Proceedings of the 20th Annual IEEEApplied Power ElectronicsConference and Exposition, APEC*, pp. 281–286, USA, March 2005.

[42] T. Dragičević, J. M. Guerrero, and J. C. Vasquez, "A distributed control strategy for coordination of an autonomous LVDC microgrid based on power-line signaling," *IEEE Transactions on Industrial Electronics*, vol. 61, no. 7, pp. 3313–3326, 2014.

[43] H. Valderrama-Blavi, J. M. Bosque, F. Guinjoan, L. Marroyo, and L. Martínez-Salamero, "Power adaptor device for domestic DC microgrids based on commercial MPPT inverters," *IEEE Transactions on Industrial Electronics*, vol. 60, no. 3, pp. 1191–1203, 2013.

[44] R. Silva-Ortigoza, V. Hernández-Guzmán, M. Antonio-Cruz, and D. Muñoz-Carrillo, "DC/DC Buck power converter as a

smooth starter for a DC motor based on a hierarchical control," *IEEE Transactions on Power Electronics*, vol. 30, no. 2, pp. 1076–1084, 2015.

[45] Y. Zhao, W. Qiao, and D. Ha, "A sliding-mode duty-ratio controller for DC/DC buck converters with constant power loads," *IEEE Transactions on Industry Applications*, vol. 50, no. 2, pp. 1448–1458, 2014.

[46] K. K. S. Leung and H. S. H. Chung, "Derivation of a second-order switching surface in the boundary control of buck converters," *IEEE Power Electronics Letters*, vol. 2, no. 2, pp. 63–67, 2004.

[47] V. Utkin, J. Guldner, and J. Shi, *Sliding Mode Control in Electromechanical Systems*, Taylor and Francis, London, U.K, 1999.

[48] J. J. E. Slotine and W. Li, *Sliding control in Applied Non-linear Control*, Prentice-Hall, Inc, Englewood Cliffs, NJ, USA, 1991.

[49] Intel. Voltage Regulator Module (VRM) and Enterprise Voltage Regulator-Down (EVRD) 11.1—Design Guidelines, Intel Corporation: Santa Clara, CA, USA, 2009.

[50] T. Wildi, *Electrical Machines, Drives and Power Systems*, Prentice Hall, Columbus, OH, USA, 6 edition, 2006, Electrical Machines, Drives and Power Systems.

[51] B. Shrestha, N. R. Bhuyan, and B. N. Sinha, *Sliding Mode Control of Switching Power Converters Technique and Implementation*, vol. 4, CRC press, Taylor & Francis Group, Boca Raton, NY, USA, 1st edition, 2012.